Photodissociation of CHF2Cl at 193 nm: H/Cl and Cl(P-2(1/2))/Cl(P-2(3/2)) branching ratios

ARTICLE *in* THE JOURNAL OF PHYSICAL CHEMISTRY A · AUGUST 1996

Impact Factor: 2.69 · DOI: 10.1021/jp9609038

7 AUTHORS, INCLUDING:

Ilana Bar
Ben-Gurion University of the Negev
172 PUBLICATIONS **2,254** CITATIONS
SEE PROFILE

S. Rosenwaks
Ben-Gurion University of the Negev
257 PUBLICATIONS **3,471** CITATIONS
SEE PROFILE

Photodissociation of CHF_2Cl at 193 nm: H/Cl and $Cl(^2P_{1/2})/Cl(^2P_{3/2})$ Branching Ratios

Aviva Melchior,* Patrick Knupfer, Ilana Bar, and Salman Rosenwaks

Department of Physics, Ben-Gurion University of the Negev, Beer-Sheva 84105, Israel

Thomas Laurent, Hans-R. Volpp, and Jürgen Wolfrum

Physikalisch-Chemisches Institut der Universität Heidelberg, Im Neuenheimer Feld 253, D-69120 Heidelberg, Germany

Received: March 21, 1996; In Final Form: May 30, 1996[⊗]

The photodissociation of chlorodifluoromethane, CHF_2Cl (HCFC-22), was studied by a laser pump-and-probe technique, using 193 nm excitation of the parent molecule and a time-of-flight mass spectrometer combined with (2 + 1) resonance-enhanced multiphoton ionization to detect products. Photolysis via two channels, C−Cl and C−H bond rupture, was observed, while HCl elimination was not found. The H, $Cl(^2P_{3/2})$ and $Cl(^2P_{1/2})$ yields are found to be first order in the photolysis and third order in the probe laser intensity. The H/Cl and $Cl(^2P_{1/2})/Cl(^2P_{3/2})$ branching ratios are 0.19 ± 0.06 and 0.36 ± 0.03, respectively. The mechanism of the dissociation is discussed in view of these results.

Introduction

Exploring the photodissociation of molecules through absorption of one or more photons has greatly contributed to our understanding of the dynamics and the mechanisms that govern the rupture of chemical bonds.[1,2] Of particular interest is photodissociation of molecules, radicals, and clusters relevant to the chemistry of the atmosphere, since it is the first step for many important chain reactions. Photodissociation studies provide information on primary photochemical channels, product branching ratios, fragment state distributions, and internal energy partitioning among the fragments and thus may help to explain the processes that occur in the atmosphere.

The present study is part of our ongoing investigation of the photodissociation and reaction dynamics of hydrochlorofluorocarbon (HCFC) and hydrofluorocarbon (HFC) compounds.[3] These species are becoming increasingly important in atmospheric chemistry owing to the imminent phase out of the ozone-destroying chlorofluorocarbons (CFC's) and halons[4−6] and their replacement by HCFC's and HFC's, which have been suggested as environmentally acceptable alternatives. The emissions of HCFC's are assumed to grow at 3% per year until 2020 with reductions to zero emissions by 2040.[5] The processes that can destroy these molecules in the troposphere and thus reduce their transport to the stratosphere are reactions with OH free radicals and photolysis. The relatively short tropospheric lifetimes (<20 years) of the HCFC's and HFC's lead to lower ozone depletion potentials and global warming potentials than in the case of CFC's and halons.[5,6]

The HCFC's possess a broad and unstructured UV absorption spectra in the 180−240 nm region, with cross sections of $\sim 10^{-19}$ cm^2 at ~180 nm that decrease by several orders of magnitude at 240 nm.[7] This absorption band is assigned as a $n \rightarrow \sigma^*$ transition where electron density is transferred from a nonbonding to an antibonding orbital localized in the C−Cl bond. The main primary photolytic process expected through absorption in this band is the rupture of the C−Cl bond.[8]

The photolysis of HCFC's has rarely been studied, although it is one of the processes that determine their atmospheric fate and is expected to release energetic and highly reactive Cl species into the atmosphere. Huber and co-workers[9] studied the photodissociation of $CHFCl_2$ (HCFC-21) at 193 nm by photofragment translational spectroscopy. They found that the primary dissociation process proceeds exclusively via the rupture of a C−Cl bond. From the measured anisotropy parameter they concluded that the photolysis of $CHFCl_2$ involves an electronic transition polarized perpendicular to the CHF molecular plane and parallel to the line connecting the two Cl atoms.

TABLE 1: Standard Enthalpies of Formation ΔH^0_f and Reaction Enthalpies ΔH^0 of Dissociation Processes of CHF_2Cl

species	ΔH^0_f (298 K) (kJ mol^{-1})	ref	reaction	ΔH^0 (298 K) (kJ mol^{-1})
CHF_2Cl	−483.7	7	$CHF_2Cl \rightarrow CHF_2 + Cl$	366.1
CHF_2	−238.9	7	$\rightarrow CF_2Cl + H$	432.7
CF_2Cl	−269.0	7	$\rightarrow CF_2 + HCl$	197.3
CHFCl	−60.76	10	$\rightarrow CClF + HF$	190.4
CF_2	−194.1	7	$\rightarrow CHFCl + F$	502.3
CHF	108.94	11	$\rightarrow CHF + ClF$	542.3
CHCl	297.49	11	$\rightarrow CHCl + F + F$	940.0
HCl	−92.31	7	$\rightarrow CHF + Cl + F$	793.3
ClF	−50.3	12	$\rightarrow CHCl + F_2$	781.2
HF	−273.3	7		
F_2	0	7		
CClF	−20	7		
Cl	121.30	7		
H	217.997	7		
F	79.39	7		

In this paper we report on the 193 nm photodissociation of chlorodifluoromethane, CHF_2Cl (HCFC-22). From the standard enthalpies of formation (ΔH^0_f), the dissociation enthalpies (ΔH^0) for CHF_2Cl are calculated and summarized in Table 1. At 193 nm (620 kJ mol^{-1}), the photodissociation channels that are energetically accessible are the first six in Table 1. We have monitored those leading to Cl, H, and HCl formation. The Cl can be obtained in both the ground $Cl(^2P_{3/2})$ and excited $Cl(^2P_{1/2})$ spin−orbit states, hereafter referred to as Cl and Cl*, respectively. Establishment of the photolytic channels and measurement of the relative yields of the products in the photodissociation of CHF_2Cl are of importance to both atmospheric chemistry and molecular dynamics. Furthermore, the measure-

* Corresponding author.

[⊗] Abstract published in *Advance ACS Abstracts,* July 15, 1996.

S0022-3654(96)00903-3 CCC: $12.00

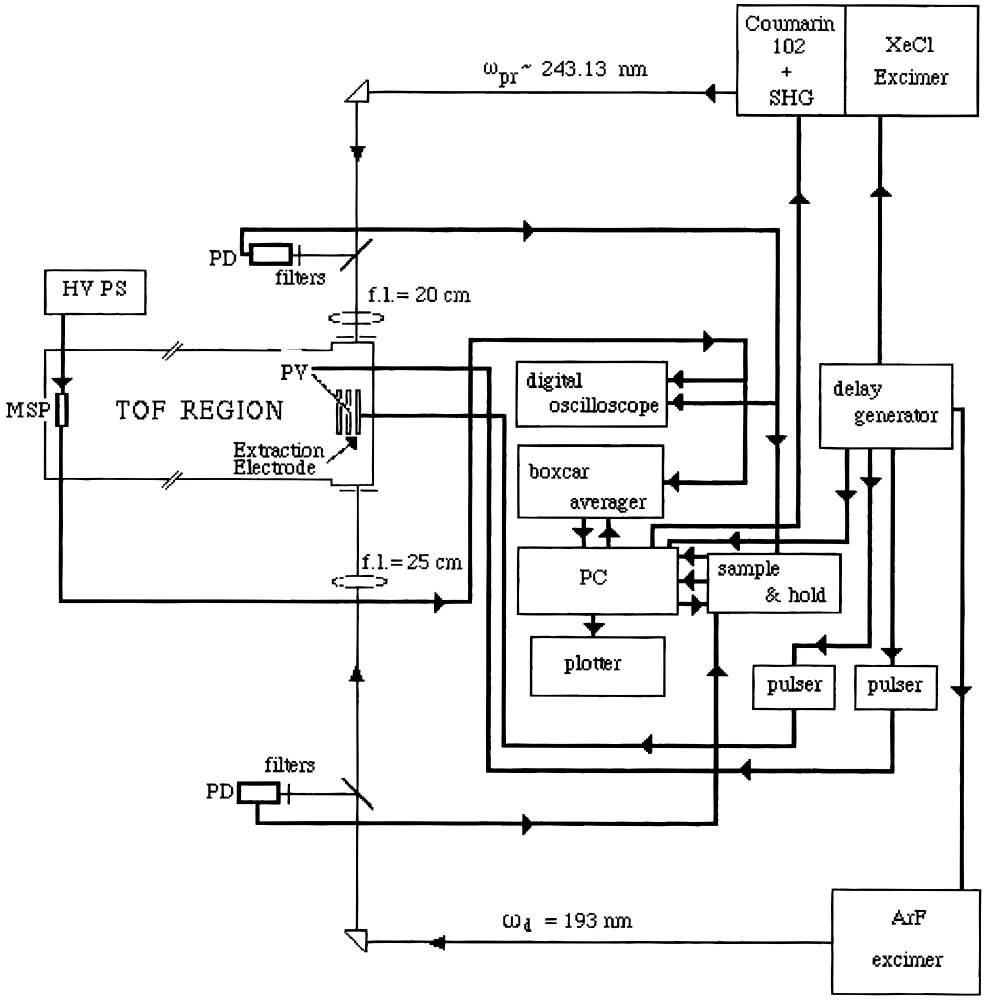

Figure 1. Schematic diagram of the experimental setup: TOF, time-of-flight; MSP, microsphere plate; PV, pulsed valve; HV PS, high-voltage power supply; PD, photodiode; SHG, second harmonic generator; f.l., focal length; ω_d, photolysis laser beam; ω_{pr}, probe laser beam.

ment of the branching ratio of the products is of considerable experimental and theoretical interest in photodissociation processes where the fragments appear in open-shell electronic states.[13−16] In such processes, more than one electronic potential energy surface (PES) correlates with a given fine structure level of one or more fragments. Therefore, measurement of the relative branching ratio into the various fragment fine-structure levels is essential to understand the couplings during the breakup of the molecular bond.

We combined (2 + 1) resonance-enhanced multiphoton ionization (REMPI) and time-of-flight mass spectrometry (TOFMS) to state-selectively monitor the H, Cl, Cl*, and HCl fragments. Only the first three species were observed. The dependence of the TOFMS signal on the intensity of the photolysis and of the probe laser, and the H/Cl and Cl/Cl* branching ratios, were determined. The mechanism of the photodissociation of CHF_2Cl is discussed in view of these results.

Experimental Section

The experiments were carried out in a home-built Wiley-McLaren TOFMS.[17] A schematic of the experimental setup is shown in Figure 1. CHF_2Cl (Atochem, 99.5%) is introduced into the ionization−extraction region through a pulsed valve (PV, General Valve, 9) and admitted via a stainless steel needle located approximately 2 mm from the center of the extraction region of the TOFMS. The source chamber is pumped by a liquid-nitrogen-trapped diffusion pump (Alcatel, Crystal 100) and the ion detector chamber is pumped by a turbomolecular pump (Alcatel, 5150). The base pressure in the source and ion detector chambers is $<10^{-7}$ Torr, and the typical pressure in the source chamber when the reagent is being admitted is 8×10^{-6} Torr (measured with Granville-Phillips 274015 and Televac II pressure gauges). The molecules cross the counterpropagating photolysis (ω_d) and probe laser (ω_{pr}) beams. They are photolyzed with an unpolarized ArF excimer laser beam at 193.3 nm (0.7 nm bandwidth, Lambda Physik, EMG 101 MSC), and the photoproducts are detected by a frequency-doubled dye laser (about 0.003 nm bandwidth, Lambda Physik, FL 3002) pumped by a XeCl excimer laser (Lambda Physik, EMG 101 MSC). Coumarin 102 dye and a BBO crystal for frequency doubling are used to cover the 234−244 nm region. The pulse duration of both beams is ~15 ns. The ω_d and ω_{pr} pulses are focused with 25 and 20 cm focal length lenses to spot sizes of about 200 and 100 μm, and their typical energies in the interaction zone are 300 and 200 μJ, respectively. These energies were chosen to ensure that the background signal originating from each laser is minimal.

The focused output of ω_{pr} is used to ionize chlorine, hydrogen, or hydrogen chloride photofragments through (2 + 1) REMPI. The fine-structure splitting of the Cl $3p^5(^2P^0; J = 1/2, 3/2)$ ground state is 881 cm^{-1}. The branching ratio of $Cl(^2P_j)$ is obtained via the two-photon transitions $4p\ ^2D_{3/2} \leftarrow 3p\ ^2P_{3/2}$ at 235.336 nm and $4p\ ^2D_{3/2} \leftarrow 3p\ ^2P_{1/2}$ at 237.808 nm.[13,18,19] All measurements are carried out for the mass-selected ^{35}Cl isotope peak. H atoms are monitored via the two-photon transition 2s

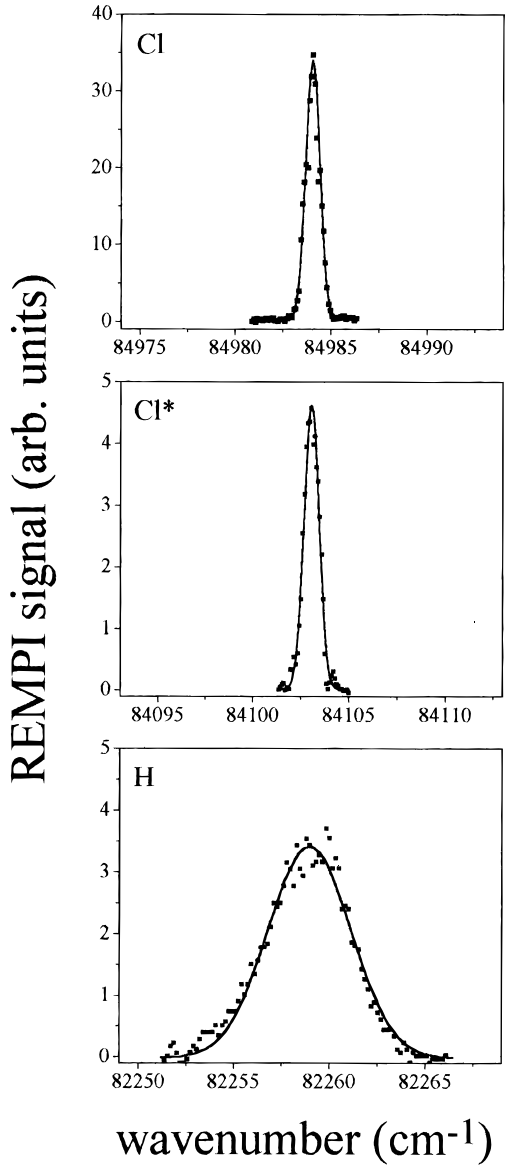

Figure 2. (2 + 1) REMPI signals of ^{35}Cl ionized via 4p $^2D_{3/2} \leftarrow$ 3p $^2P_{3/2}$, $^{35}Cl^*$ via 4p $^2D_{3/2} \leftarrow$ 3p $^2P_{1/2}$, and H via the 2s $^2S \leftarrow$ 1s ^2S transition following 193 nm photolysis of CHF_2Cl.

$^2S \leftarrow$ 1s ^2S at 243.135 nm[13,19] and HCl molecules via the $V^1\Sigma^+ \leftarrow X^1\Sigma^+$, $E^1\Sigma^+ \leftarrow X^1\Sigma^+$ two-photon transitions in the 235−239 nm region.[20,21] The dependence of the H and Cl ion signals on the intensity of the photolysis or the probe laser is measured using attenuators. The delay between ω_d and ω_{pr} is controlled by a delay generator (Stanford Research Systems, DG535). Delays in the range 0−40 ns were tried, and the optimal Cl^+ and H^+ signals were found to be around 5 ns. The short delay ensures that collisions of the photolysis products prior to detection are negligible. All measurements were carried out at a repetition rate of 10 Hz.

The ions are formed in the ionization region behind a pulsed extractor (kept at about −300 V) and accelerated by two plates kept at −1250 and − 2500 V, respectively. The ions pass through two pairs of orthogonal steering plates (2400 ± 100 V) before entering the TOF tube (−2500 V, 106 cm long). After passing through a focusing ring, the ions are detected by a microsphere plate (MSP, El-Mul, Z033). The output of the detector is amplified and fed into a digital oscilloscope (Gould 4072) interfaced to a personal computer (PC). Wavelength-dependent mass spectra of selected ion peaks are acquired using a boxcar integrator (Stanford Research Systems, SR250 and SR280). The ion signal and the signals from two photodiodes (PD, Hamamatsu, S-1336 Q) that monitor the energy of ω_{pr} and ω_d are passed to the PC. Each data point in the ensuing spectra is obtained from these signals as an average of 30 pulses.

Results and Discussion

Figure 2 displays the REMPI profiles of ^{35}Cl, $^{35}Cl^*$, and H, following the photodissociation of CHF_2Cl at 193 nm. It indicates that a significant yield of hydrogen atoms is obtained during the dissociation process. Despite the effort made to detect HCl fragments, it was not observed. From the signal-to-noise ratio in a sample of neat HCl, the upper limit for the HCl elimination channel in the 193 nm photodissociation of CHF_2Cl is estimated to be <1%.

Figure 2 also shows that the widths of Cl and Cl* profiles are much smaller than that of the H atom fragment. The width of the profile reflects the contributions of the fragment translational energy, the internal energy of the parent molecule, and the bandwidths of the lasers. For C−Cl bond rupture the available energy (E_{avl}) is 253.9 kJ mol^{-1} (Table 1) but the departing, heavy Cl atom is slow and the line width of the Cl fragments REMPI signals is governed by the probe laser bandwidth**.** The maximum width of the H profile agrees with that calculated from E_{avl} (187.3 kJ mol^{-1}) assuming that all of it is converted into translational energy. Furthermore, comparison of this profile width to those resulting from the 193 nm photodissociation of HCl, in our system as well as in ref 22, shows that they are quite similar. This similarity is consistent with the fact that E_{avl} for H−Cl (188.4 kJ mol^{-1}) and $CClF_2$−H bond ruptures, in one-photon photolysis at 193 nm, are almost identical.

The dependences of the H and ^{35}Cl REMPI signals on the intensity of the pump laser are displayed in panels a and b of Figure 3. The slopes of the log−log plots are 0.9 ± 0.2 and 0.9 ± 0.1, respectively, as expected for a one-photon process. As shown in panels c and d of Figure 3, the corresponding slopes for the probe laser are 3.2 ± 0.3 and 3.0 ± 0.3, which are consistent with the three-photon nature of the REMPI process. Similar dependences were obtained for the Cl* fragment. The one-photon dependence on the pump and three-photon on the probe are consistent with the following sequences:

$$CHF_2Cl \rightarrow CHF_2/CF_2Cl + Cl(Cl^*)/H \quad (1)$$

followed by

$$Cl\ (^2P_{3/2},^2P_{1/2}) \rightarrow Cl\ (^2D_{3/2}) \quad (2)$$

$$Cl\ (^2D_{3/2}) \rightarrow Cl^+ \quad (3)$$

and in case an H atom is formed in (1),

$$H\ (1s\ ^2S) \rightarrow H\ (2s\ ^2S) \quad (4)$$

$$H\ (2s\ ^2S) \rightarrow H^+ \quad (5)$$

One may argue that the CHF_2/CF_2Cl radicals formed in (1) could further photodissociate:

$$CHF_2 \rightarrow CF_2 + H \quad (6)$$

$$CF_2Cl \rightarrow CF_2 + Cl \quad (7)$$

Another possibility is the sequence

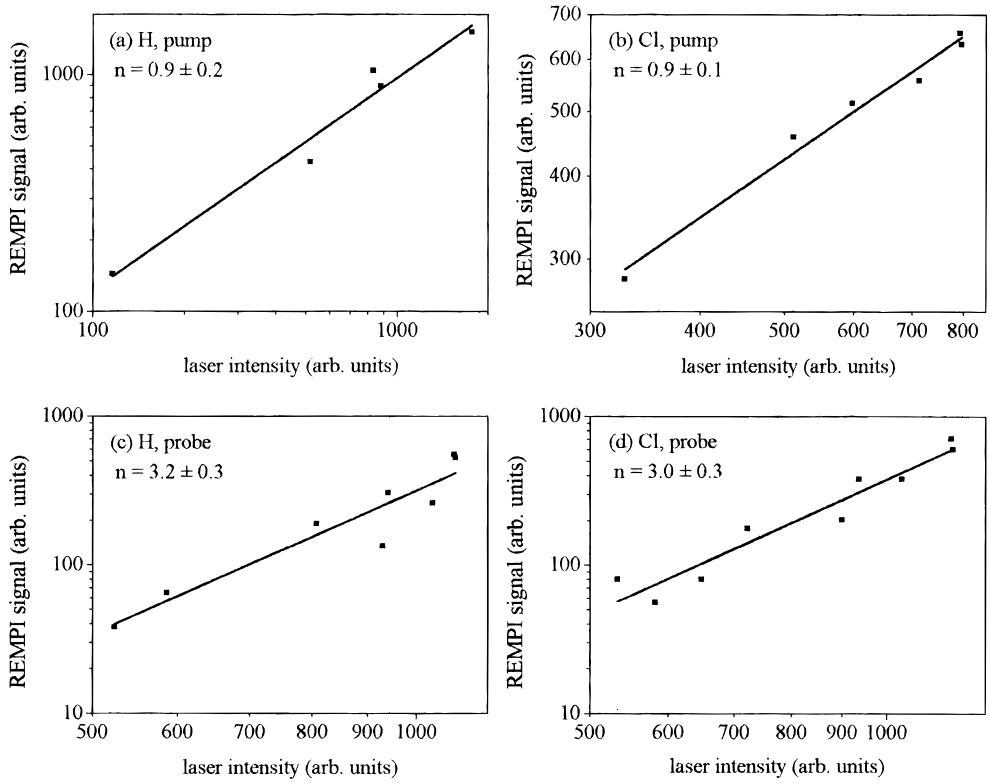

Figure 3. Dependence of the H and ^{35}Cl REMPI signals on pump [(a) and (b)] and probe [(c) and (d)] laser intensity. Each point in the plot represents an average of 50 data points.

$$CHF_2Cl \rightarrow CHFCl + F \quad (8)$$

$$CHFCl \rightarrow CHF/CFCl + Cl/H \quad (9)$$

However, the sequences 1, 6 and 1, 7 or 8, and 9 would not lead to the observed intensity dependences unless one of the photolysis steps is saturated. The low intensity of ω_d minimizes saturation and multiphoton photolysis processes. Also, in the formation of CHF_2 and CF_2Cl radicals (eq 1) the maximal internal energies they can acquire are <253.9 and <187.3 kJ mol^{-1}, respectively (Table 1). These energies are lower than the threshold energies for secondary dissociation of the above radicals, 262.8 and 196.2 kJ mol^{-1}, respectively. Therefore, in the absence of collisions the nascent radicals CHF_2 and CF_2Cl are stable. From this analysis and from the width of the H profile it can be concluded that the Cl, Cl*, and H atoms are primary products of the one-photon absorption of CHF_2Cl.

The Cl*/Cl branching ratio was obtained from the ratio of the integrated areas under their REMPI profiles, corrected for the respective two-photon oscillator strength. The ratio of the oscillator strengths was determined[13a] to be $f(^2D_{3/2} \leftarrow {}^2P_{3/2})/f(^2D_{3/2} \leftarrow {}^2P_{1/2}) = 2.5$. By use of this value, the Cl*/Cl branching ratio is given by

$$[Cl^*]/[Cl] = 2.5 \times S_{Cl^*}/S_{Cl} \quad (10)$$

where S_{Cl^*} and S_{Cl} denote the integrated areas for the Cl* ($^2D_{3/2} \leftarrow {}^2P_{1/2}$) and Cl ($^2D_{3/2} \leftarrow {}^2P_{3/2}$) transitions, and is found to be 0.36 ± 0.03. The $(^2P_{1/2})/(^2P_{3/2})$ branching ratios measured for the molecule studied here and several other halogen-containing compounds are given in Table 2. The branching ratios spread from very low values up to values close to 1 depending on the compound and the photodissociating wavelength, which determine the dissociation mechanism.

The interpretation of spin−orbit branching ratios is difficult without the availability of reasonable dynamical calculations, and therfore, it can be done only qualitatively. The two main factors determining the branching ratio of spin−orbit states of an atomic fragment in photodissociation processes are the structure of the excited state wave function in the Franck−Condon region where photodissociation is initiated and the couplings between different PES at large distances where the separation between the molecular states is close to the fragment spin−orbit splitting. The adiabaticity parameter[2,13,16]

TABLE 2: $X(^2P_{1/2})/X(^2P_{3/2})$ (X = Cl, I) Branching Ratios Following the Photodissociation of Several Molecules at Various Wavelengths

molecule	ω_d (nm)	X*/X	ref
HCl	193	0.50 ± 0.07	13a[a]
	157	0.83 ± 0.11	13a[a]
	143−167	0.50−0.63	16
DCl	193	0.21 ± 0.08	13a[a]
	157	0.28 ± 0.08	13a[a]
HI	266	0.67	23
ICl X = Cl	235−238	0.68 ± 0.10	24
ICl X = I	248	0.71 ± 0.27	24
Cl_2	308	< 0.025	25[b]
CH_3Cl	193	0.59 ± 0.14	13a[a]
CH_2Cl_2	193	0.37 ± 0.15	13a[a]
CCl_4	193	0.28 ± 0.08	13a[a]
CHF_2Cl	193	0.36 ± 0.03	*c*
t-CHClCHCl	193	0.15 ± 0.03	14b
	214	0.26 ± 0.02	26
	220	0.41 ± 0.23	26
cis-CHClCHCl	214	0.23 ± 0.08	26
	220	0.32 ± 0.22	26
CH_2CCl_2	193	0.28 ± 0.05	14b
	214	0.64 ± 0.04	26
	220	0.83 ± 0.27	26
CH_2CHCl	193	0.30 ± 0.05	14b

[a] Average calculated from the values given in Table 2 of ref 13a. [b] Ratio is calculated by multiplying the signal intensity ratio reported in the (2 + 1) REMPI measurement by the factor 2.5, as explained in the text. [c] This work.

$$\xi = R\Delta E_{so}/(v\hbar) \quad (11)$$

where R is the width of the recoupling region, ΔE_{so} is the spin−orbit splitting, and v is the recoil velocity, gives the ratio of the recoil time to the spin−orbit precession period. Thus, if this parameter is large, adiabatic correlation of the fragment atomic spin−orbit states with the excited molecular states is anticipated, while if it is small, i.e., the fragments recoil fast, we expect a diabatic distribution.

Following estimates for R in similar cases,[13b,16] we choose R in the range of 1.5−4.0 bohr. v is taken to be 4900 m s^{-1} (assuming that all the available energy is converted to fragment translation). ξ is then in the range 2.4−6.8, which is consistent with adiabatic behavior. The observed Cl*/Cl branching may be attributed to excitation of several molecular states, where each of the atomic spin−orbit states adiabatically correlates to at least one excited molecular state. A similar situation is found in the photodissociation of HI at 266 nm where the ground state is excited both to the $^3\Pi_0^+$ state that generates exclusively $I(^2P_{1/2})$ and to the $^3\Pi_1$ state that forms $I(^2P_{3/2})$.[13b,23]

The branching ratio of the channels leading to the Cl and H fragments was obtained from the ratio of the Cl ($^2D_{3/2} \leftarrow {}^2P_{3/2}$) and H (2s $^2S \leftarrow$ 1s ^2S) REMPI signals multiplied by the ratio of detection sensitivity for these transitions. The last ratio was obtained from the REMPI signal ratio for the 193 nm photodissociation of HCl, $S_H/S_{Cl} = 4.2 \pm 0.7$.[19] This value is similar to that measured in our system for the photodissociation of HCl at 193 nm. Comparing this value to the known population ratio of H to Cl ($^2P_{3/2}$) in the photodissociation of HCl,[13a] we obtain the relation

$$[H]/[Cl] = (0.36 \pm 0.06) \times S_H/S_{Cl} \quad (12)$$

Therefore, the H/Cl branching ratio for the photodissociation of CHF_2Cl is given by

$$[H]/[Cl]_{total} = [H]/\{1.32([Cl] + [Cl^*])\} = [H]/\{1.32 \times 1.36[Cl]\} = 0.36S_H/\{1.32 \times 1.36S_{cl}\} \quad (13)$$

where the factor 1.32 accounts for the relative abundance of the two chlorine isotopes (since S_H/S_{Cl} in eq 12 is given[19] for naturally abundant Cl while in eq 13 for ^{35}Cl). The integrated areas under the REMPI profiles for the photodissociation of CHF_2Cl give the ratio $S_H/S_{Cl} = 0.95 \pm 0.10$. Consequently, the branching ratio is 0.19 ± 0.06.

In contrast to the appreciable amount of H atoms produced in the photolysis of CHF_2Cl, Huber and co-workers[9] did not find any evidence for C−H bond fission in their study of the 193 nm photodissociation of $CHFCl_2$. They attempted to detect the counterfragment of the H atom, $CFCl_2$, by photofragment translational spectroscopy using a low-velocity molecular beam and a small laboratory scattering angle (8°). Under these conditions and after extensive signal accumulation, no signal was detected. Since they also did not observe Cl_2 and HCl, or their counterfragments CHF and CFCl, respectively, they concluded that $CHFCl_2$ decays exclusively via a single C−Cl bond rupture.

As mentioned above, we could not find any evidence for HCl fragments in the 193 nm photolysis of CHF_2Cl. In contrast, HCl elimination was obtained as a minor pathway of ethyl chloride (CH_3CH_2Cl) photolysis[27] at 193 nm and as a substantial channel of dissociation of vinyl chloride (CH_2═$CHCl$) and dichloroethylenes (CH_2═CCl_2 and CHCl═CHCl).[26,28] The formation of HCl has been attributed to an indirect mechanism that involves radiationless conversion from the initially excited state to the ground state.[26−28] The fact that HCl elimination does not occur in the photodissociation of methane derivatives, although it is energetically more favorable than the C−Cl bond fission, implies that the dissociation takes place on a strongly repulsive PES that is not coupled efficiently with the electronic ground state.[9]

Conclusions

In this study three channels of CHF_2Cl photodissociation at 193 nm were investigated. C−Cl bond fission was found to be the main channel, but C−H bond cleavage is a significant channel as well. The HCl elimination channel is negligible. The Cl*/Cl branching ratio and the estimated adiabaticity parameter imply that the Cl fragments are formed by an adiabatic process that involves more than one excited molecular state. Further photodissociation studies of CHF_2Cl and other HCFC's at this and additional wavelengths will give a better understanding of these processes.

Understanding the dynamics of CHF_2Cl and other HCFC's photodissociation is not only of fundamental importance but also crucial for revealing their ozone depletion and global-warming potentials. These parameters are calculated from the atmospheric lifetimes, obtained from the UV photolysis absorption cross section and from the rate constants for reactions with OH.[29,30] We believe that future modeling should take into account, in addition to the absorption cross section, the different photodissociation channels and their branching ratios to assess more accurately the atmospheric impact of HCFC's.

Acknowledgment. This research was supported by the Israeli Academy of Science and Humanities and the European Community and The Israel Ministry of Sciences and Arts under Contract No. CI1*-CT94-0096 and by the James Franck Binational German-Israeli Program in Laser-Matter Interaction. T.L. thanks the DAAD-Bonn for a travel grant. We are very grateful to Professor P.J. Dagdigian for valuable discussions and to Dr. P. Marcus for technical advice during the construction of the TOFMS.

References and Notes

(1) Schinke, R. *Photodissociation Dynamics Spectroscopy and Fragmentation of Small Polyatomic Molecules*; Cambridge University Press: Cambridge, 1993.

(2) Levine, R. D.; Bernstein, R. B. *Molecular Reaction Dynamics and Chemical Reactivity*; Oxford University Press: Oxford, 1987.

(3) Laurent, T.; Lillich, H.; Volpp, H.-R.; Wolfrum, J.; Bar, I.; Melchior, A.; Rosenwaks, S. *Chem. Phys. Lett.* **1995**, *247*, 321.

(4) Rowland, F. S. *Environ. Sci. Technol.* **1991**, *25*, 622.

(5) McFarland, M.; Kaye, J. *Photochem. Photobiol.* **1992**, *55*, 911.

(6) Scientific Assessment of Ozone Depletion: 1991. World Meteorological Organization Global Research and Monitoring Project Report No. 25; World Meteorological Organization: Geneva, Switzerland, 1992.

(7) Atkinson, R.; Baulch, D. L.; Cox, R. A.; Hampson, R. F., Jr.; Kerr, J. A.; Troe, J. *J. Phys. Chem. Ref. Data* **1992**, *21*, 1125.

(8) Okabe, H. *Photochemistry of Small Molecules*; John Wiley & Sons: New York, 1978.

(9) Yang, X.; Felder, P.; Huber, J. R. *Chem. Phys.* **1994**, *189*, 129.

(10) Tschuikow-Roux, E.; Paddison, S. *Int. J. Chem. Kinet.* **1987**, *19*, 15.

(11) Lias, S. G.; Karpas, Z.; Liebman, J. F. *J. Am. Chem. Soc.* **1985**, *107*, 6089.

(12) *CRC Handbook of Chemistry and Physics*, 74th ed.; Lide, D. R., Ed.; CRC Press: Boca Raton, Florida, 1993−1994.

(13) (a) Tonokura, K.; Matsumi, Y.; Kawasaki, M.; Tasaki, S.; Bersohn, R. *J. Chem. Phys.* **1992**, *97*, 8210. (b) Matsumi, Y.; Tonokura, K.; Kawasaki, M.; Ibuki, T. *J. Chem. Phys.* **1990**, *93*, 7981. (c) Matsumi, Y.; Tonokura, K.; Kawasaki, M. *J. Chem. Phys.* **1992**, *97*, 1065.

(14) (a) Huang, Y.; Yang, Y.-A.; He, G.; Hashimoto, S.; Gordon, R. J. *J. Chem. Phys.* **1995**, *103*, 5476. (b) Mo, Y.; Tonokura, K.; Matsumi, Y.; Kawasaki, M.; Sato, T.; Arikawa, T.; Reilly, P. T. A.; Xie, Y.; Yang, Y.; Huang, Y.; Gordon, R. J. *J. Chem. Phys.* **1992**, *97*, 4815.

(15) Alexander, M. H.; Pouilly, B.; Duhoo, T. *J. Chem. Phys.* **1993**, *99*, 1752.

(16) Liyanage, R.; Yang, Y.; Hashimoto, S.; Gordon, R. J.; Field, R. W. *J. Chem. Phys.* **1995**, *103*, 6811.
(17) Wiley, W. C.; McLaren, I. H. *Rev. Sci. Instrum.* **1955**, *26*, 1150.
(18) Arepalli, S.; Presser, N.; Robie, D.; Gordon, R. J. *Chem. Phys. Lett.* **1985**, *118*, 88.
(19) Matsumi, Y.; Tonokura, K.; Kawaski, M.; Tsuji, K.; Obi, K. *J. Chem. Phys.* **1993**, *98*, 8330.
(20) Callaghan, R.; Arepalli, S.; Gordon, R. J. *J. Chem. Phys.* **1987**, *86*, 5273.
(21) Varley, D. F.; Dagdigian, P. J. *J. Phys. Chem.* **1995**, *99*, 9843.
(22) Koppe, S.; Laurent, T.; Naik, P. D.; Volpp, H.-R.; Wolfrum, J.; Arusi-Parpar, T.; Bar, I.; Rosenwaks, S. *Chem. Phys. Lett.* **1993**, *214*, 546.
(23) Schmiedl, R.; Dungan, H.; Meir, W.; Welge, K. H. *Z. Phys.* **1982**, *A304*, 137.
(24) Tonokura, K.; Matsumi, Y.; Kawasaki, M.; Kim, H. L.; Yabushita, S.; Fujimura, S.; Saito, K. *J. Chem. Phys.* **1993**, *99*, 3461.
(25) Matsumi, Y.; Kawasaki, M.; Sato, T.; Kinugawa, T.; Arikawa, T. *Chem. Phys. Lett.* **1989**, *155*, 486.
(26) Sato, K.; Shihira, Y.; Tsunashima, S.; Umemoto, H.; Takayanagi, T.; Furukawa, K.; Ohno, S. *J. Chem. Phys.* **1993**, *99*, 1703.
(27) Kawasaki, M.; Kasatani, K.; Sato, H.; Shinohara, H.; Nishi, N. *Chem. Phys.* **1984**, *88*, 135.
(28) Umemoto, M.; Seki, K.; Shinohara, H.; Nagashima, U.; Nishi, N.; Kinoshita, M.; Shimada, R. *J. Chem. Phys.* **1985**, *83*, 1657.
(29) Talukdar, R.; Mellouki, A.; Gierczak, T.; Burkholder, J. B.; McKeen, S. A.; Ravishankara, A. R. *Science* **1991**, *252*, 693.
(30) Solomon, S.; Mills, M.; Heidt, L. E.; Pollock, W. H.; Tuck, A. F. *J. Geophys. Res.* **1992**, *97*, 825.

JP9609038